Chapter 4

Chiral Perturbation Theory and the δ-regime

As it was mentioned in Chapter 2, the low energy regime of QCD cannot be treated with perturbation theory, but one can use lattice simulations. The most successful analytic approach to this regime is *Chiral Perturbation Theory*, which is an effective field theory. In virtue of the chiral symmetry breaking of QCD, the Lagrangian of the effective theory is built by introducing a field in the coset space of the symmetry breaking group. This field describes the lightest particles of QCD, since at low energy they dominate the theory. If the symmetry breaking is spontaneous, the particles that appear are massless and they are known as Nambu-Goldsone Bosons. On the other hand, if the symmetry breaking is explicit, the particles have a light mass and we refer to them as quasi Nambu-Goldstone Bosons. The effective Lagrangian must contain all the terms that are consistent with the symmetries of the underlying theory. This leads to a consideration of the chiral symmetry of the QCD Lagrangian.

4.1 QCD chiral symmetry

Since we are interested in low energy, we will work with the flavors whose masses satisfy $m_f \ll \Lambda_{\text{QCD}} \approx 300$ MeV. Therefore we only take into account the u and d quarks, with masses in the following range [1]

$$\begin{aligned} m_u &= 1.9 \text{ - } 2.65 \text{ MeV}, \\ m_d &= 4.5 \text{ - } 5.15 \text{ MeV}. \end{aligned} \tag{4.1}$$

Then, in Minkowski space-time, the QCD Lagrangian is given by

$$\begin{aligned} \mathcal{L} &= \sum_{f=u,d} (\overline{q}_f i\gamma^\mu D_\mu q_f - m_f \overline{q}_f q_f) - \frac{1}{4}\text{tr}\left[G_{\mu\nu}G^{\mu\nu}\right], \\ D_\mu &= (\partial_\mu + igA_\mu), \;\; G_{\mu\nu} = \partial_\mu A_\nu - \partial_\nu A_\mu + ig[A_\mu, A_\nu], \end{aligned} \tag{4.2}$$

where q_f and $\overline{q}_f$ are Grassmann fields associated with the flavor f with mass m_f and where the gauge field is $A_\mu(x) = \sum_{a=1}^{8} A_\mu^a(x) T_a$, where $A_\mu^a(x)$ are field components and T_a are the basis elements of the traceless Hermitian 3×3 matrices (generators of SU(3)). This implies that the gauge field is a matrix as well. The Lagrangian is constructed in the same way as we did in Section 2.3, so it is invariant under SU(3) gauge transformations. We are interested in analyzing the chiral symmetry, therefore we apply the chiral projection operators

$$P_R = \frac{1}{2}(\mathbb{I} + \gamma_5), \;\; P_L = \frac{1}{2}(\mathbb{I} - \gamma_5), \tag{4.3}$$

to the quark fields in order to obtain the right-handed and left-handed fields

$$q_{R_f} = P_R q_f, \;\; q_{L_f} = P_L q_f, \;\; \overline{q}_{R_f} = \overline{q}_f P_L, \;\; \overline{q}_{L_f} = \overline{q}_f P_R. \tag{4.4}$$

By using $\{\gamma_5, \gamma^\mu\} = 0$, $\gamma_5^2 = \mathbb{I}$, $\gamma_5^\dagger = \gamma_5$ and the definition (4.3) of the chiral operators one can show the following properties

$$P_{L,R} = P_{L,R}^\dagger, \;\; P_{L,R}^2 = P_{L,R}, \;\; P_R P_L = P_L P_R = 0, \;\; P_{R,L}\gamma^\mu = \gamma^\mu P_{L,R}, \tag{4.5}$$

$$q_f = q_{R_f} + q_{L_f}, \quad \overline{q}_f = \overline{q}_{R_f} + \overline{q}_{L_f}. \tag{4.6}$$

With eqs. (4.5) and eqs. (4.6) the QCD Lagrangian takes the form

$$\mathcal{L} = \sum_{f=u,d} \left[\overline{q}_{L_f} i\gamma^\mu D_\mu q_{L_f} + \overline{q}_{R_f} i\gamma^\mu D_\mu q_{R_f} - m_f(\overline{q}_{R_f} q_{L_f} + \overline{q}_{L_f} q_{R_f}) \right] - \frac{1}{4}\mathrm{tr}\left[G_{\mu\nu}G^{\mu\nu}\right]. \tag{4.7}$$

Now, we use global chiral transformations defined by

$$q_{R,L_f} \to q'_{R,L_f} = e^{i\alpha\gamma_5} q_{R,L_f}, \;\; \overline{q}_{R,L_f} \to \overline{q}'_{R,L_f} = \overline{q}_{R,L_f} e^{i\alpha\gamma_5}, \;\; \alpha \in \mathbb{R}. \tag{4.8}$$

By using $\gamma^\mu e^{i\alpha\gamma_5} = e^{-i\alpha\gamma_5}\gamma^\mu$, the quark part of the Lagrangian transforms as

$$\begin{aligned} &\sum_{f=u,d} \left[\left(\overline{q}'_{L_f} i\gamma^\mu D_\mu q'_{L_f} + \overline{q}'_{R_f} i\gamma^\mu D_\mu q'_{R_f} \right) - m_f(\overline{q}'_{R_f} q'_{L_f} + \overline{q}'_{L_f} q'_{R_f}) \right] \\ &= \sum_{f=u,d} \left[\left(\overline{q}_{L_f} i\gamma^\mu D_\mu q_{L_f} + \overline{q}_{R_f} i\gamma^\mu D_\mu q_{R_f} \right) - m_f(\overline{q}_{R_f} e^{i2\alpha\gamma_5} q_{L_f} + \overline{q}_{L_f} e^{i2\alpha\gamma_5} q_{R_f}) \right] \end{aligned} \tag{4.9}$$

Hence, $\mathcal{L}$ is invariant under the transformations of eq. (4.8) only when $m_f = 0$, for that reason this is called the chiral limit. Let us work in the chiral limit for the moment.

If we express the quark fields as doublets

$$q_{R,L} = \begin{pmatrix} q_{R,L_u} \\ q_{R,L_d} \end{pmatrix}, \;\; \overline{q}_{R,L} = \left(\overline{q}_{R,L_u}, \overline{q}_{R,L_d} \right), \;\; q = \begin{pmatrix} q_u \\ q_d \end{pmatrix}, \;\; \overline{q} = \left(\overline{q}_u, \overline{q}_d \right), \tag{4.10}$$

we can rewrite the massless Lagrangian as

$$\mathcal{L} = \overline{q}_L i\gamma^\mu D_\mu q_L + \overline{q}_R i\gamma^\mu D_\mu q_R - \frac{1}{4}\mathrm{tr}\left[G_{\mu\nu}G^{\mu\nu}\right] \tag{4.11}$$

and apply separate global U(2) transformations

$$\begin{aligned} q_R \to q'_R = R\, q_R, \quad \overline{q}_R \to \overline{q}'_R = \overline{q}_R R^\dagger, \quad R \in \mathrm{U}(2)_R, \\ q_L \to q'_L = L\, q_L, \quad \overline{q}_L \to \overline{q}'_L = \overline{q}_L L^\dagger, \quad L \in \mathrm{U}(2)_L. \end{aligned} \tag{4.12}$$

Under these transformations, $\mathcal{L}$ is once again invariant. The corresponding symmetry group is $\mathrm{U}(2)_L \otimes \mathrm{U}(2)_R$. An element of U(2) can be decomposed into an element of SU(2) multiplied by a phase factor, thus

$$\mathrm{U}(2)_L \otimes \mathrm{U}(2)_R = \mathrm{SU}(2)_L \otimes \mathrm{SU}(2)_R \otimes \mathrm{U}(1)_B \otimes \mathrm{U}(1)_A, \tag{4.13}$$

where $\mathrm{U}(1)_A$ is the axial symmetry, which is broken explicitly under quantization (axial anomaly). $\mathrm{U}(1)_B$ is associated with the baryon number conservation, while $\mathrm{SU}(2)_L \otimes$

$\mathrm{SU}(2)_R$ is the chiral symmetry group. The latter breaks spontaneously to SU(2). We analyze this through the chiral condensate

$$\langle 0|\,\overline{q}q\,|0\rangle = \langle 0|\,(\overline{q}_R q_L + \overline{q}_L q_R)\,|0\rangle\,. \tag{4.14}$$

Under the transformations in eq. (4.12) the chiral condensate transforms as

$$\langle 0|\,\overline{q}'q'\,|0\rangle = \langle 0|\,(\overline{q}_R R^\dagger L q_L + \overline{q}_L L^\dagger R q_R)\,|0\rangle\,, \tag{4.15}$$

where we see that $\langle 0|\,\overline{q}q\,|0\rangle$ remains invariant only if $R = L$. Hence, we have the following spontaneous breaking pattern

$$\mathrm{SU}(2)_L \otimes \mathrm{SU}(2)_R \to \mathrm{SU}(2)_{L=R}. \tag{4.16}$$

The order parameter of this broken symmetry is $\langle 0|\,\overline{q}q\,|0\rangle$, so when it is different from zero the chiral symmetry is indeed spontaneously broken. Because of the Goldstone theorem, this broken symmetry corresponds to

$$\dim(\mathrm{SU}(2)_L \otimes \mathrm{SU}(2)_R) - \dim(\mathrm{SU}(2)) = 3 + 3 - 3 = 3 \tag{4.17}$$

massless Nambu-Goldstone Bosons (NGB). If now we take into account the masses m_u and m_d, the symmetry is explicitly broken and the NGBs turn into light massive quasi NGBs, which can be identified with the pion triplet π^+, π^-, π^0. See refs. [2–4] for extensive reviews.

4.2 Effective Lagrangian

In order to build the effective Lagrangian $\mathcal{L}_{\text{eff}}$, one introduces a field $U(x)$ in the coset space of the symmetry breaking group, *i.e.*

$$U(x) \in (\mathrm{SU}(2)_L \otimes \mathrm{SU}(2)_R)/\mathrm{SU}(2)_{L=R} = \mathrm{SU}(2), \tag{4.18}$$

which transforms under global transformations of $\mathrm{SU}(2)_L \otimes \mathrm{SU}(2)_R$ as

$$U(x) \to U'(x) = RU(x)L^\dagger, \;\; R \in \mathrm{SU}(2)_R, \;\; L \in \mathrm{SU}(2)_L. \tag{4.19}$$

This field is expressed in terms of dynamical variables suitable for low-energy. For two quark flavors this means that one replaces the quark and gluon fields by pseudo-scalar pion fields: $\vec{\pi} = \{\pi_1(x), \pi_2(x), \pi_3(x)\}$. Thus, $U(x)$ is written as

$$U(x) = \exp\left(i\frac{\vec{\pi}\cdot\vec{\tau}}{F_\pi}\right), \;\; \vec{\tau} = (\sigma_1, \sigma_2, \sigma_3), \tag{4.20}$$

where F_π is known as the pion decay constant and makes the argument of the exponential dimensionless (the pion fields have dimension of mass in units of $c = \hbar = 1$ in $d = 4$) and where σ_i are the Pauli matrices, which are the generators of SU(2). Hence

$$U(x) = \exp\left(i\frac{\phi(x)}{F_\pi}\right), \;\; \phi(x) = \begin{pmatrix} \pi^0 & \sqrt{2}\pi^+ \\ \sqrt{2}\pi^- & -\pi^0 \end{pmatrix},$$
$$\pi^0 = \pi_3, \;\; \pi^\pm = \frac{\pi_1 \mp i\pi_2}{\sqrt{2}}. \tag{4.21}$$

$\mathcal{L}_{\text{eff}}$ is constructed by using $U(x)$. It must have all the terms that present the symmetries of QCD, in particular Lorentz invariance and chiral symmetry. Each term is accompanied by a coefficient denominated Low Energy Constant (LEC), which is a free parameter of the

theory and has to be determined from the underlying theory. However, there are actually an infinite number of terms consistent with the symmetries. They can be organized in increasing powers of momentum, which is the same as increasing number of derivatives, so one can truncate them for low energy. In the massless case, the effective Lagrangian with the least number of derivatives reads

$$\mathcal{L}_{\text{eff}} = \frac{F_\pi^2}{4}\text{tr}\left(\partial_\mu U \partial^\mu U^\dagger\right). \tag{4.22}$$

The factor $F_\pi^2/4$ is written because if one expands in powers of ϕ up to second order, the kinetic term $\frac{1}{2}\text{tr}(\partial_\mu\phi\partial^\mu\phi^\dagger)$ is obtained. Under the transformation of eq. (4.19) the Lagrangian is invariant

$$\mathcal{L}_{\text{eff}} = \frac{F_\pi^2}{4}\text{tr}\left(\Omega_R\partial_\mu U\Omega_L^{-1}\Omega_L\partial^\mu U^\dagger\Omega_R^{-1}\right) = \frac{F_\pi^2}{4}\text{tr}\left(\Omega_R^{-1}\Omega_R\partial_\mu U\partial^\mu U^\dagger\right) = \frac{F_\pi^2}{4}\text{tr}\left(\partial_\mu U\partial^\mu U^\dagger\right), \tag{4.23}$$

where we have used the cyclic property of the trace.

If one introduces the masses m_u and m_d to the theory, a term that explicitly breaks the chiral symmetry is added

$$\mathcal{L}_{\text{s.b.}} = \frac{F_0^2 B_0}{2}\text{tr}\left(MU^\dagger + UM\right), \quad M = \begin{pmatrix} m_u & 0 \\ 0 & m_d \end{pmatrix}, \tag{4.24}$$

where s.b. stands for "symmetry breaking" and F_0 and B_0 are two LECs. To leading order the massive effective Lagrangian reads

$$\mathcal{L}_{\text{eff}} = \frac{F_\pi^2}{4}\text{tr}\left(\partial_\mu U\partial^\mu U^\dagger\right) + \frac{F_0^2 B_0}{2}\text{tr}\left(MU^\dagger + UM\right). \tag{4.25}$$

For degenerate quark masses, $m_u = m_d \equiv m$, the LECs satisfy the following relations [5]

$$\begin{aligned} F_\pi &= F_0\left[1 + O\left(\frac{m}{\Lambda_{\text{QCD}}}\right)\right], \\ \langle 0|\,\bar{q}q\,|0\rangle &= -2F_0^2 B_0\left[1 + O\left(\frac{m}{\Lambda_{\text{QCD}}}\right)\right], \\ m_\pi &= \sqrt{2B_0 m}\left[1 + O\left(\frac{m}{\Lambda_{\text{QCD}}}\right)\right]. \end{aligned} \tag{4.26}$$

In the chiral limit $F_\pi = F_0$. For $m \ll \Lambda_{\text{QCD}}$ eqs. (4.26) allow us to write $\mathcal{L}_{\text{eff}}$ in a more convenient way

$$\mathcal{L}_{\text{eff}} = \frac{F_\pi^2}{4}\text{tr}\left(\partial_\mu U\partial^\mu U^\dagger\right) + \frac{\Sigma}{4}\text{tr}\left(MU^\dagger + UM\right), \quad \Sigma \equiv -\langle 0|\,\bar{q}q\,|0\rangle. \tag{4.27}$$

The effective Lagrangian can be formulated in terms of a normalized field $\vec{S}(x) \in \text{O}(4)$, $|\vec{S}(x)| = 1$ as well, since there is a local isomorphism between O(4) and $\text{SU}(2)_L \otimes \text{SU}(2)_R$. This is known as the non-linear σ model [6]. The symmetry breaking pattern takes the form

$$\text{O}(4) \to \text{O}(3) \quad \longleftrightarrow \quad \text{SU}(2)_L \otimes \text{SU}(2)_R \to \text{SU}(2). \tag{4.28}$$

In terms of the field $\vec{S}(x)$, the $\mathcal{L}_{\text{eff}}$ term with the least number of derivatives reads

$$\mathcal{L}_{\text{eff}} = \frac{F_\pi^2}{2}\partial^\mu\vec{S}\cdot\partial_\mu\vec{S}. \tag{4.29}$$

Now, we introduce an external field $\vec{H}$ that explicitly breaks the symmetry by adding the term

$$\mathcal{L}_{\text{s.b.}} = -\Sigma\vec{H}\cdot\vec{S}, \tag{4.30}$$

where $\vec{H}$ plays the same role as the degenerate quark mass.

4.3 Regimes of Chiral Perturbation Theory

From eq. (4.25) we see that the leading order LECs are F_π, B_0 and F_0. These constants can be determined through lattice QCD simulations. Still, one cannot simulate an infinite volume, so three regimes with finite volume in Euclidean space, $V = L^3 \times L_t$, have been established. For each one of them, the relation between the LECs can be different from the one that is shown in eqs. (4.26). Nevertheless, the value of the LECs is the same in all the regimes. Let us briefly review them:

- The *p-regime* consists of a large volume compared to the correlation length: $L, L_t \gg \xi = m_\pi^{-1}$. In this regime the finite volume corrections are suppressed by a factor proportional to $\exp(-m_\pi L)$, so eqs. (4.26) are valid [5].
- If $L, L_t \lesssim \xi$ we refer to the *ϵ-regime* [7]. Here the finite volume corrections cannot be neglected. In the ϵ-regime the chiral condensate has the following dependence on the LECs, m and the volume when $B_0 m L^2 \ll 1$ (see ref. [8])

$$\langle 0|\,\overline{q}q\,|0\rangle = -2F_0^2 B_0 \left(\frac{I_1'(F_0^2 B_0 m V)}{I_1(F_0^2 B_0 m V)} - \frac{1}{F_0^2 B_0 m V}\right), \tag{4.31}$$

  where I_1 is the modified Bessel function of first kind of order one. Let us revise the infinite volume limit of this expression. For that purpose, we denote $x = F_0^2 B_0 m V$ and we use the asymptotic large x form of the modified Bessel functions (see e.g. ref. [9])

$$I_\nu(x) \sim \frac{e^x}{\sqrt{2\pi x}}\left(1 - \frac{4\nu^2 - 1}{8x}\right). \tag{4.32}$$

  Then

$$\frac{I_1'(x)}{I_1(x)} - \frac{1}{x} \sim -\frac{15 - 30x + 16x^2}{6x - 16x^2}. \tag{4.33}$$

  When $x \to \infty$ this expression converges to 1. Thus, the infinite volume limit of eq. (4.31) recovers $\langle 0|\,\overline{q}q\,|0\rangle = -2F_0^2 B_0$. On the other hand, we obtain the limit of $\langle 0|\,\overline{q}q\,|0\rangle$ when $m \to 0$ at finite volume. To do so we use the following expressions for the modified Bessel functions and their derivatives

$$I_\nu(x) = \sum_{k=0}^{\infty} \frac{(x/2)^{\nu+2k}}{k!\Gamma(\nu + k + 1)}, \quad I_\nu'(x) = I_{\nu-1}(x) - \frac{\nu}{x} I_\nu(x). \tag{4.34}$$

  Then we have

$$\begin{aligned} \frac{I_1'}{I_1} - \frac{1}{x} \quad &= \quad \frac{I_0(x) - \frac{1}{x} I_1(x)}{I_1(x)} - \frac{1}{x} = \frac{\sum_{k=0}^{\infty} \frac{(x/2)^{2k}}{k!\Gamma(k+1)}}{\sum_{l=0}^{\infty} \frac{(x/2)^{1+2l}}{l!\Gamma(l+2)}} - \frac{2}{x} \\ &\underbrace{\approx}_{x \to 0} \quad \frac{\frac{1}{\Gamma(1)}}{\frac{(x/2)}{\Gamma(2)}} - \frac{2}{x} = 0. \end{aligned} \tag{4.35}$$

  Hence, we see that in the chiral limit $\langle 0|\,\overline{q}q\,|0\rangle$ vanishes. This is consistent with the fact that in finite volume there is no spontaneous symmetry breaking.
- Finally, the *δ-regime* is determined by a volume of size $V = L^3 \times L_t$, where the spatial volume is small, but the Euclidean time extent is large, that is $L \lesssim \xi \ll L_t$ [10].

The pion decay constant has been calculated in the p-regime and the ϵ-regime with three flavors several times, giving a result of $F_\pi = 92.1(9)$ MeV [11–14]. On the other hand, the δ-regime is less explored; there F_π has been measured with two flavors obtaining $F_\pi = 78^{+14}_{-10}$ MeV [15].

The ϵ and δ-regime are useful from a technical point of view, because the small volume reduces the computing time of the simulations. In particular, in the δ-regime the fact that $L \lesssim \xi \ll L_t$ has several effects. First, in the chiral limit the pion does not become massless and instead there is a *residual mass* $m_\pi^R \neq 0$ (this is also true for the ϵ-regime). Another consequence is that there is approximately only one dimension, that enables us to treat the system as a quasi one dimensional field theory, *i.e.* quantum mechanics [10]. Then, since O(4) is locally isomorphic to SU(2)⊗SU(2), if we consider again $\vec{S}(x) \in \mathrm{O}(4)$, it is possible to describe the system as a particle moving in a unit 3-sphere $\mathbb{S}^3$. One can express m_π^R as the energy gap of a quantum rotor, which is given by

$$E_j = \frac{j(j+N-2)}{2\Theta}, \tag{4.36}$$

where Θ is the moment of intertia and N refers to the group O(N). The value of Θ was computed in ref. [16] up to next-to-leading order, for a general dimension $d > 2$ and $N \geq 2$

$$\Theta = F_\pi^2 L^{d-1}\left[1 + \frac{N-2}{4\pi F_\pi^2 L^{d-2}}\left(2\frac{d-1}{d-2} + \cdots\right)\right], \tag{4.37}$$

however, the leading term had been calculated in ref. [10] for four dimensions already.

The residual pion mass is obtained by substituting $j = 1$ and $N = 4$ in eq. (4.36)

$$m_\pi^R = \frac{3}{2\Theta}. \tag{4.38}$$

In four dimensions we have

$$m_\pi^R = \frac{3}{2F_\pi^2 L^3(1+\Delta)}, \;\; \Delta = \frac{0.477\cdots}{(F_\pi L)^2} + \ldots, \;\; d = 4. \tag{4.39}$$

Calculations of Δ up to $1/(F_\pi L)^4$ have been done in ref. [17]. In two dimensions there is a divergence of the next-to-leading term, so instead we just consider the leading term, yielding

$$m_\pi^R \simeq \frac{3}{2F_\pi^2 L}, \;\; d = 2. \tag{4.40}$$

This dimension has not been considered in this context, because there are no NGBs [18–20]. Still, at finite fermion mass the lightest particles are similar to quasi NGBs and we will refer to them as pions [21]. Note that when $d = 2$, F_π is dimensionless, since the mass has units of inverse of length.

We performed simulations of the two flavor Schwinger model in the δ-regime with the HMC algorithm. This allowed us to obtain m_π^R as a function of L, in order to verify the relation $m_\pi^R \propto 1/L$ and extract the value of F_π from eq. (4.40).

4.4 δ-regime results

As in Chapter 3, we will denote $\beta = 1/g^2$. All the plots shown are in lattice units, *i.e.* the lattice constant a is set to 1. To make the lattice finer, we increment the value of β. Results for $\beta = 2, 3$ and 4 were obtained through 10^3 measurements, separated by 10 sweeps. 500 sweeps were performed to thermalize the field configurations. It is important to mention that under gauge interaction the mass of the Wilson fermion undergoes renormalization, so it is necessary to measure a renormalized mass m, instead of using the input mass of the simulations. This can be achieved with the *Partial Conservation of Axial Current* (PCAC) relation (see e.g. Section 9.1.4 of [22])

$$\langle \partial_\mu A_\mu^a(x) P^a(0)\rangle = 2m\langle P^a(x) P^a(0)\rangle, \tag{4.41}$$

where A^a_μ is the *isovector axial current*, P^a is the *pseudoscalar density* and m the renormalized fermion mass

$$A^a_\mu(x) = \frac{1}{2}\overline{q}(x)\gamma_\mu\gamma_5\sigma^a q(x),$$
$$P^a(x) = \frac{1}{2}\overline{q}(x)\gamma_5\sigma^a q(x), \tag{4.42}$$

where σ^a denotes the Pauli matrices. Equation (4.41) partially restores the broken axial symmetry when $m = 0$. With the PCAC relation, we were able to measure the renormalized fermion mass m for different lattice sizes, and thus to express m_π as a function of m.

In figure 4.1 (a), m_π is shown as a function of the degenerate quark mass m for $L = 6$, $L_t = 64$ and $\beta = 4$. We see that close to the chiral limit, the value of m_π becomes very unstable, so one cannot simply measure m_π at $m = 0$. Instead one extrapolates the value to $m = 0$. However, that is easier to do with figure 4.1 (b), where m_π is plotted against $(m^2g)^{1/3}$. A function of the form $y = \sqrt{a + b\,x^3}$, where $x = (m^2g)^{1/3}$ and a and b are fit parameters, was fitted to extrapolate to m^R_π. Many attempts with functions of the form $y = \sqrt{a + b\,x^c}$ and $y = a + bx^c$ were performed. The best results were obtained by taking $c = 3$ in the former expression. We do not have an explanation for this behavior, but it works best to infer m^R_π. We observe that in figure 4.1 (a) there are results for negative fermion mass. In the simulation both signs of the mass are measured, but the negative values do not have physical meaning and they were ignored in the extrapolations.

This same procedure was performed for different L between 5 and 12 and $L_t = 64$. In figure 4.2 we show plots of m_π vs. $(m^2g)^{1/3}$ for $\beta = 2$, in figure 4.3 for $\beta = 3$ and in figure 4.4 for $\beta = 4$.

Finally, we plot m^R_π as a function of L and fit a function of the form $3/(2LF^2_\pi)$, see figures 4.5, 4.6 and 4.7.

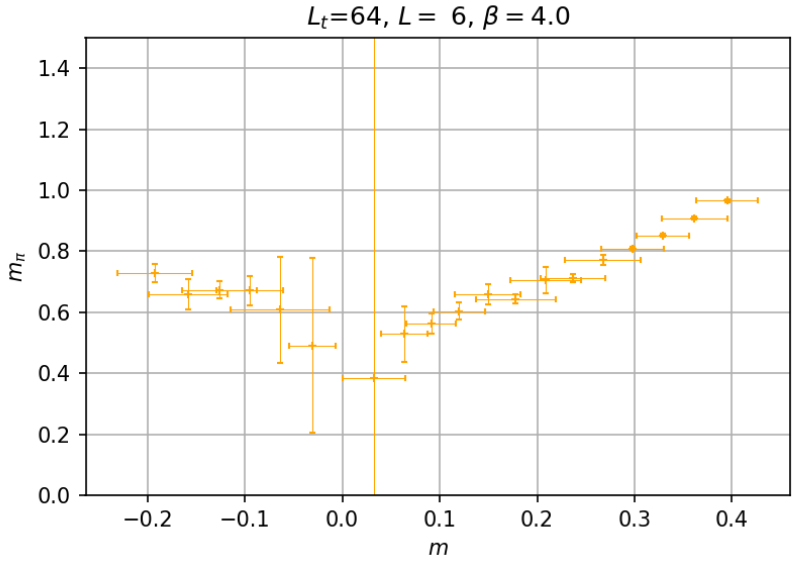

(a) m_π vs. m. We see that near $m = 0$ the pion mass result is plagued by large errors.

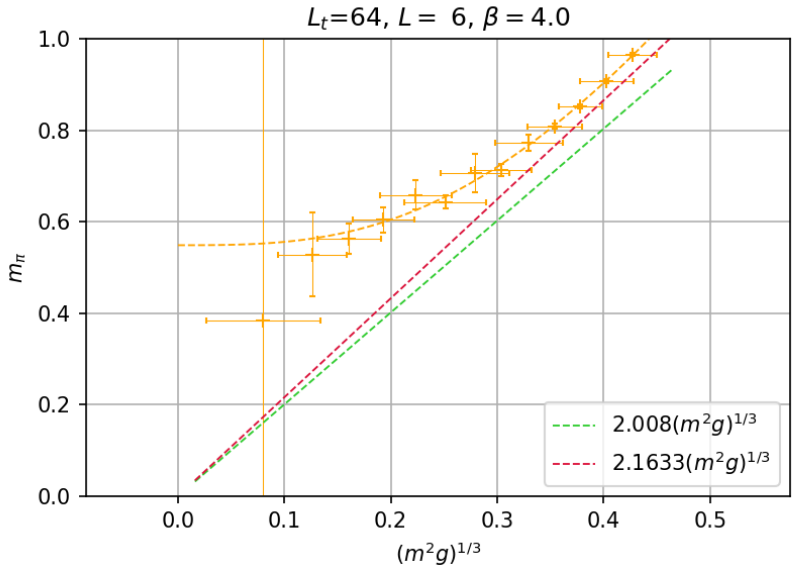

(b) m_π vs. $(m^2g)^{1/3}$. We fit a function of the form $y = \sqrt{a + bm^2g}$ to obtain the value of the residual pion mass: $m_\pi^R = 0.549(12)$. The predictions for m_π at finite temperature, mentioned in Chapter 3, are shown as well.

Figure 4.1: Results of m_π and m. Note that there are also values for $m < 0$, they are unphysical. However, in the simulation both signs of the mass are measured. In the lower plot only $m > 0$ was considered. The errors were computed by using the *jackknife method*, see Appendix C.

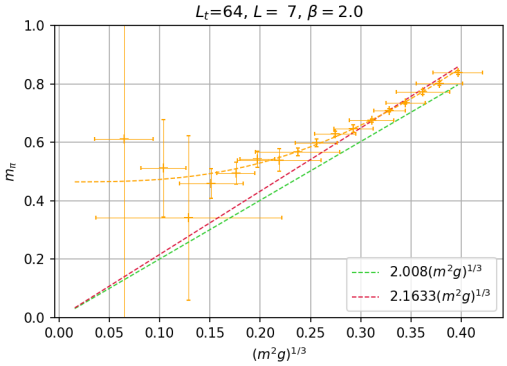

(a) m_π vs. $(m^2g)^{1/3}$ for $L = 7$. m_π =0.4645(72)

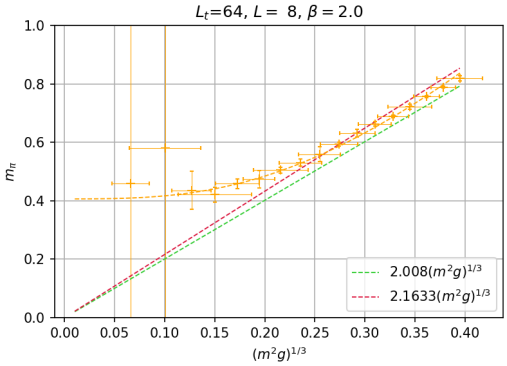

(b) m_π vs. $(m^2g)^{1/3}$ for $L = 8$. m_π =0.4063(45)

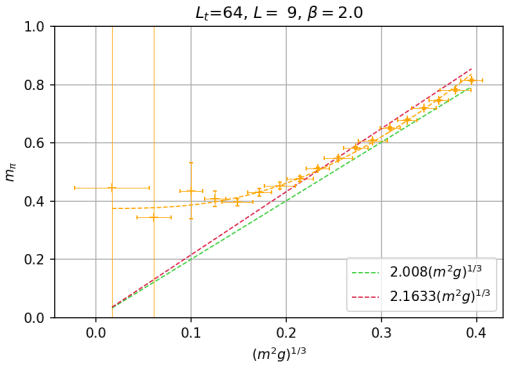

(c) m_π vs. $(m^2g)^{1/3}$ for $L = 9$. m_π =0.3749(47)

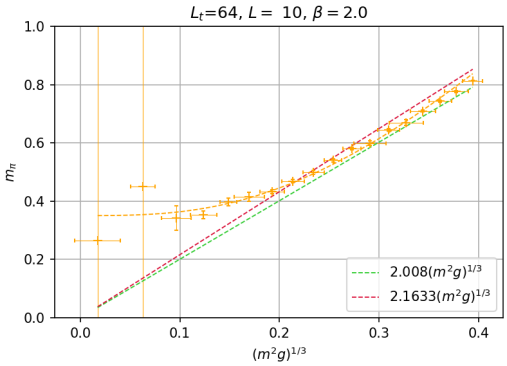

(d) m_π vs. $(m^2g)^{1/3}$ for $L = 10$. m_π =0.3505(58)

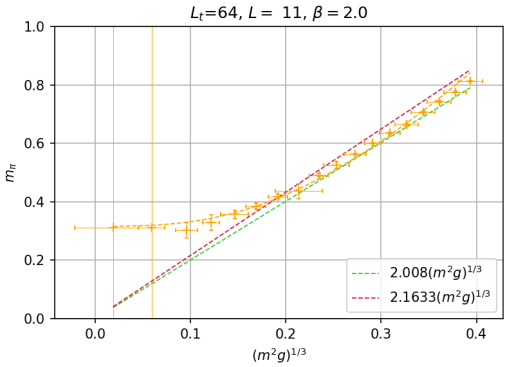

(e) m_π vs. $(m^2g)^{1/3}$ for $L = 11$. m_π =0.3163(59)

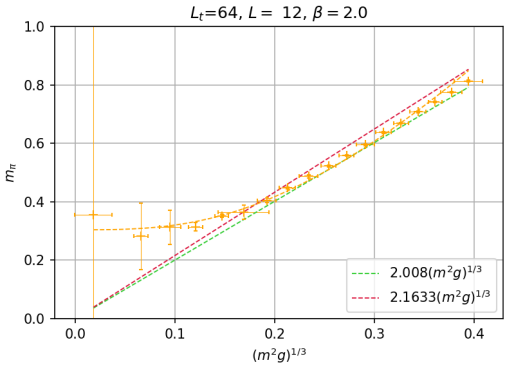

(f) m_π vs. $(m^2g)^{1/3}$ for $L = 12$. m_π =0.3040(51)

Figure 4.2: Results for $\beta = 2$. Each value of m_π and m was obtained by averaging 10^3 measurements of different configurations. Between each configuration used, 10 sweeps were performed. All the fits were made with gnuplot.

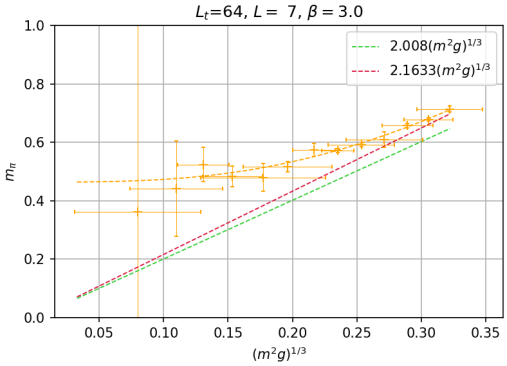

(a) m_π vs. $(m^2g)^{1/3}$ for $L = 7$. m_π =0.4639(103)

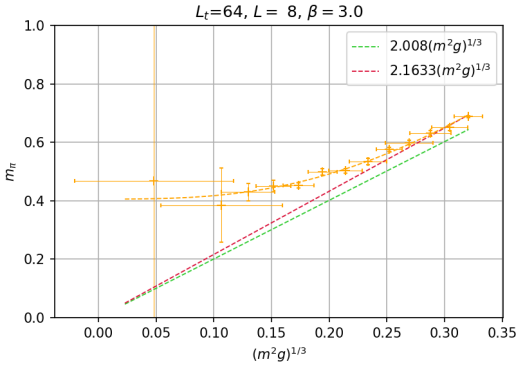

(b) m_π vs. $(m^2g)^{1/3}$ for $L = 8$. m_π =0.4057(58)

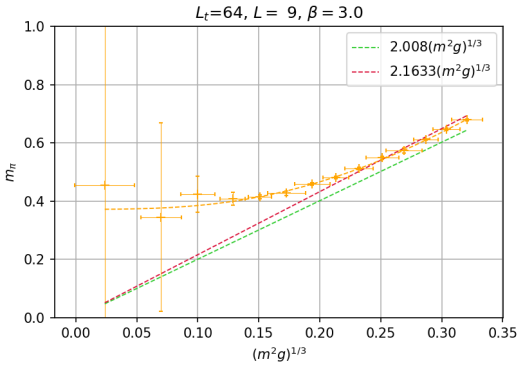

(c) m_π vs. $(m^2g)^{1/3}$ for $L = 9$. m_π =0.3722(29)

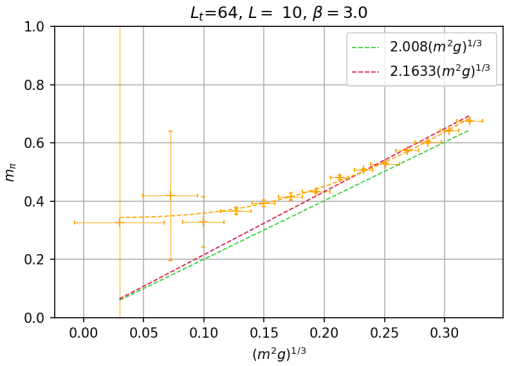

(d) m_π vs. $(m^2g)^{1/3}$ for $L = 10$. m_π =0.3437(42)

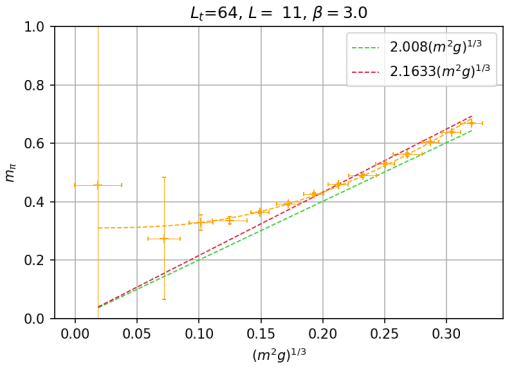

(e) m_π vs. $(m^2g)^{1/3}$ for $L = 11$. m_π =0.3104(30)

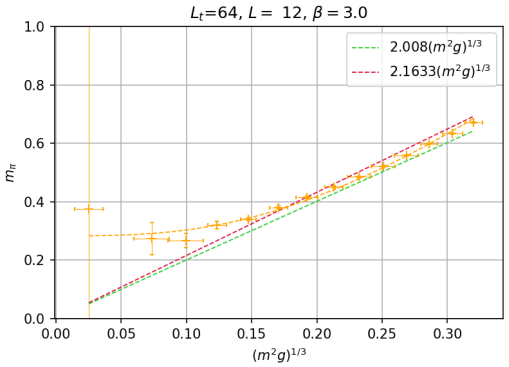

(f) m_π vs. $(m^2g)^{1/3}$ for $L = 12$. m_π =0.2832(51)

Figure 4.3: Results for $\beta = 3$. Each value of m_π and m was obtained by averaging 10^3 measurements of different configurations. Between each configuration used, 10 sweeps were performed.

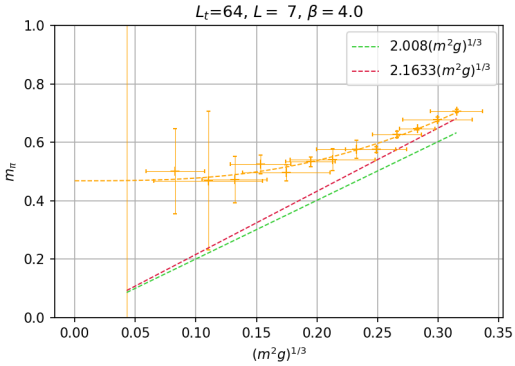

(a) m_π vs. $(m^2g)^{1/3}$ for $L = 7$. m_π =0.4684(75)

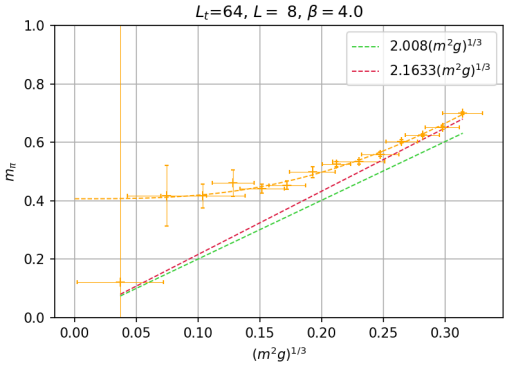

(b) m_π vs. $(m^2g)^{1/3}$ for $L = 8$. m_π =0.4068(63)

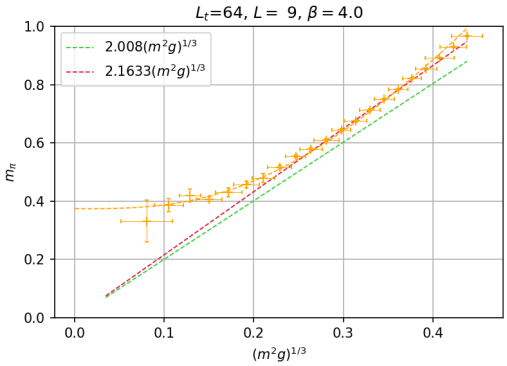

(c) m_π vs. $(m^2g)^{1/3}$ for $L = 9$. m_π =0.3741(40)

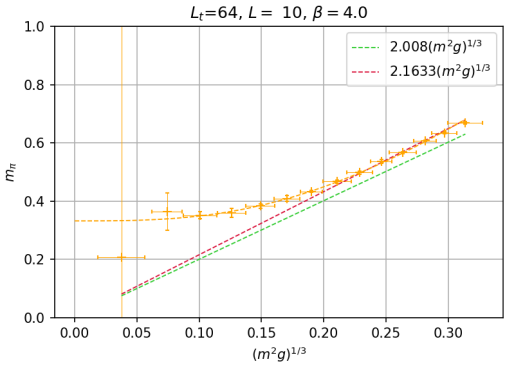

(d) m_π vs. $(m^2g)^{1/3}$ for $L = 10$. m_π =0.3323(22)

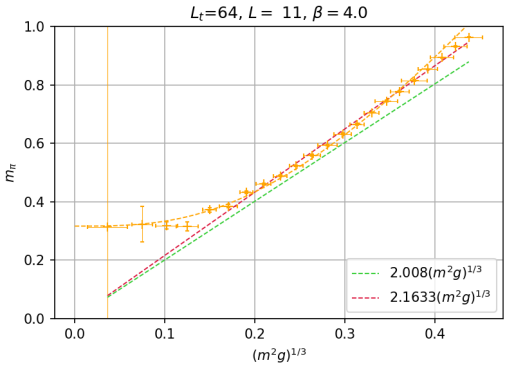

(e) m_π vs. $(m^2g)^{1/3}$ for $L = 11$. m_π =0.3167(54)

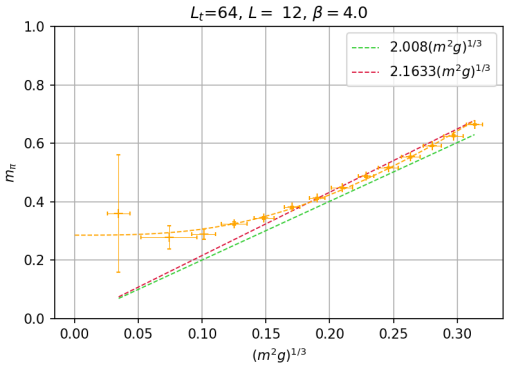

(f) m_π vs. $(m^2g)^{1/3}$ for $L = 12$. m_π =0.2857(41)

Figure 4.4: Results for $\beta = 4$. Each value of m_π and m was obtained by averaging 10^3 measurements of different configurations. Between each configuration used, 10 sweeps were performed.

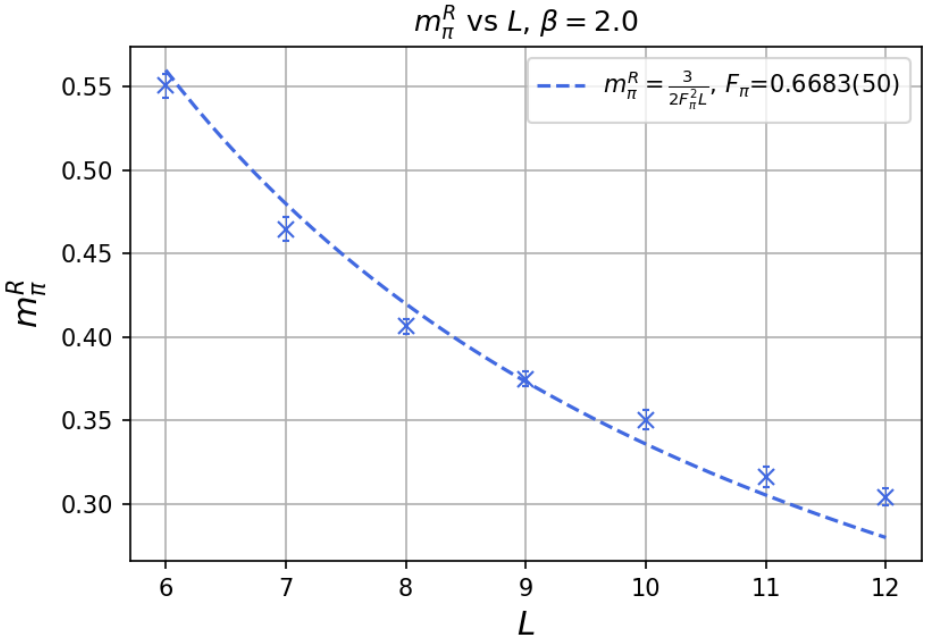

Figure 4.5: Behavior of m_π^R vs. L for $\beta = 2$.

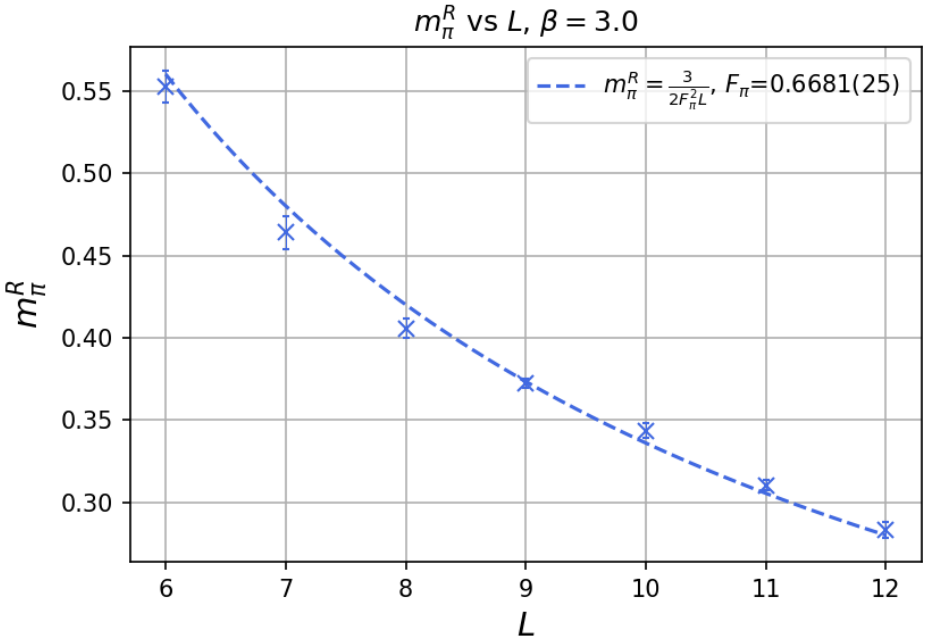

Figure 4.6: Behavior of m_π^R vs. L for $\beta = 3$.

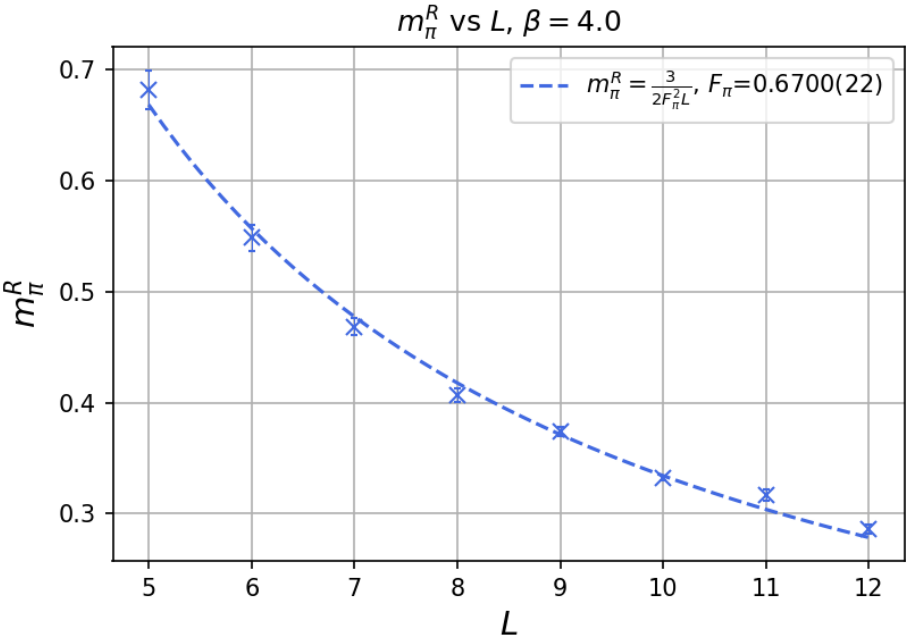

Figure 4.7: Behavior of m_π^R vs. L for $\beta = 4$. We can see that it matches the relation of $1/L$ described in eq. (4.40).

From figures 4.5, 4.6 and 4.7 we see that indeed $m_\pi^R \propto 1/L$, as we conjectured for the δ-regime. This can be best seen for $\beta = 4$, because the lattice is finer than for $\beta = 2, 3$ and as a consequence there are less lattice artifacts. Still, for $\beta = 2, 3$ the $1/L$ relation is noticeable. For all the β's used, we see that when L becomes large, m_π^R vanishes, as it should do for an infinite volume. From the fits we were able to extract F_π (see table 4.1).

β	2	3	4
F_π	0.6683(50)	0.6681(25)	0.6700(22)

Table 4.1: Pion decay constant for different values of β.

For $\beta = 4$ the error is smaller. Again, this is due to the fact that there are less lattice artifacts. An average of the values obtained for F_π yields

$$F_\pi = 0.6688(5). \tag{4.43}$$

We also measured the topological charge Q (see Chapter 5 for a definition). In figures 4.8, 4.9 and 4.10 we show the number of Monte Carlo configurations sorted according to each topological sector, for simulations with different masses. We see that the distribution of Q obeys approximately a Gaussian relation and is compatible with $\langle Q \rangle = 0$. This confirms that the simulations have been performed correctly. The exponential autocorrelation time τ_{exp} and the integrated autocorrelation time τ_{int} with respect to Q (figures 4.11, 4.12 and 4.13) were measured as well (see Appendix D for definitions). In some plots (e.g. figures 4.12 (b), (c), (e), (f) and 4.13 (d), (f)) we see that close to $m = 0$, the autocorrelation time has a peak. In some other plots, τ_{exp} and τ_{int} are scattered. We also observe that in general τ_{int} is more stable than τ_{exp}, since the procedure to measure it is more systematic and does not rely on a fit.

For $\beta = 4$, τ_{exp} and τ_{int} reach maximum values beyond 14, which points out that for finer lattices the number of sweeps between each measurement should be increased in order

to suppress correlations; although that also increases significantly the computing time of the simulations.

For $\beta = 2$, the autocorrelation time does not have a peak and in most cases it is below 2.5, which is a good sign of decorrelation. In some few cases, the exponential autocorrelation time reaches values larger than 2.5, for instance in figure 4.11 (a) and (b). In those situations, it is very likely that τ_{exp} was not properly determined by fitting eq. (D.2).

For $\beta = 3$, τ_{exp} and τ_{int} increase close to $m = 0$, but their maximum values remain below 4.

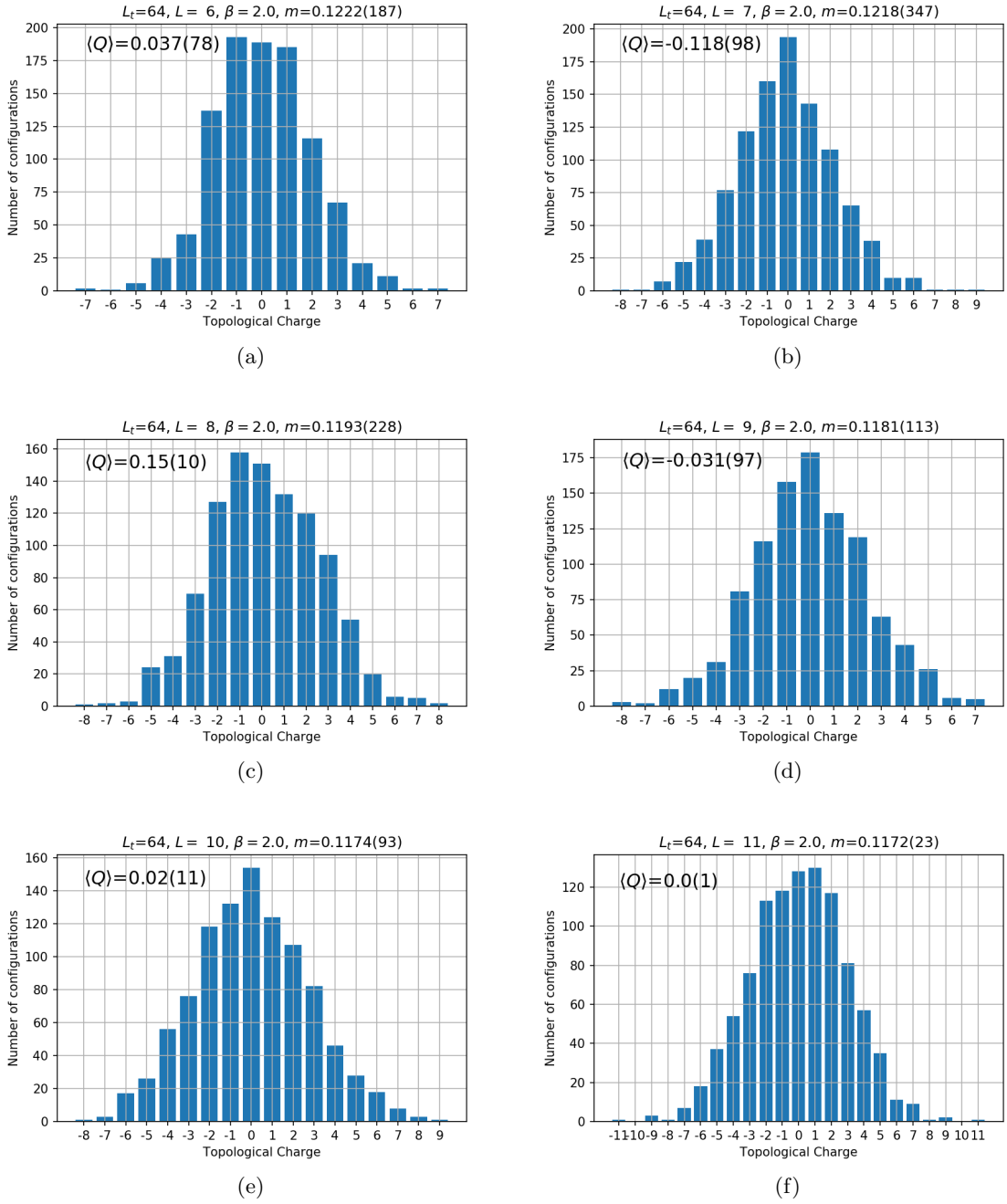

Figure 4.8: Topological charge distribution for different lattices and fermion mass, $\beta = 2$.

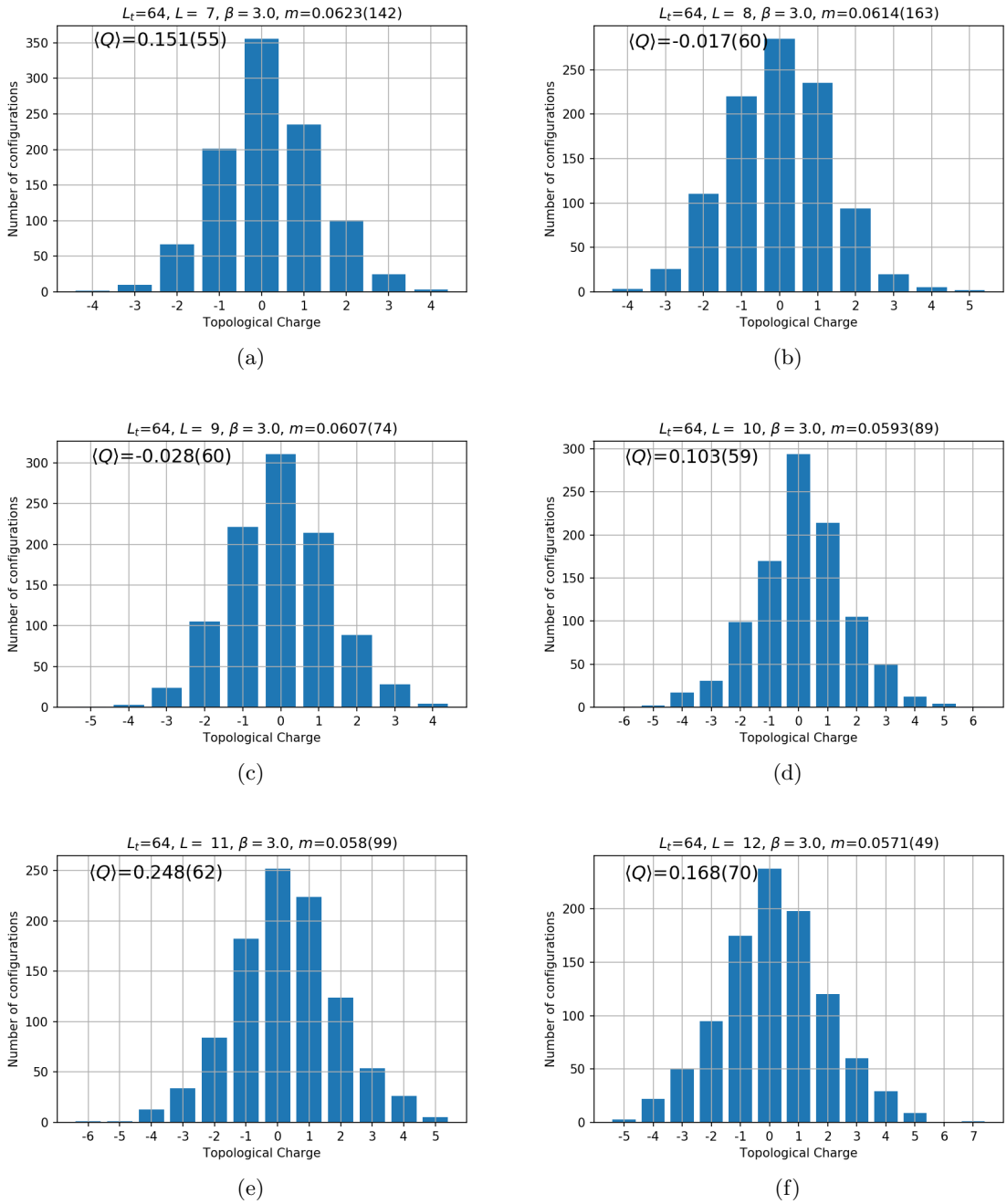

Figure 4.9: Topological charge distribution for different lattices and fermion mass, $\beta = 3$.

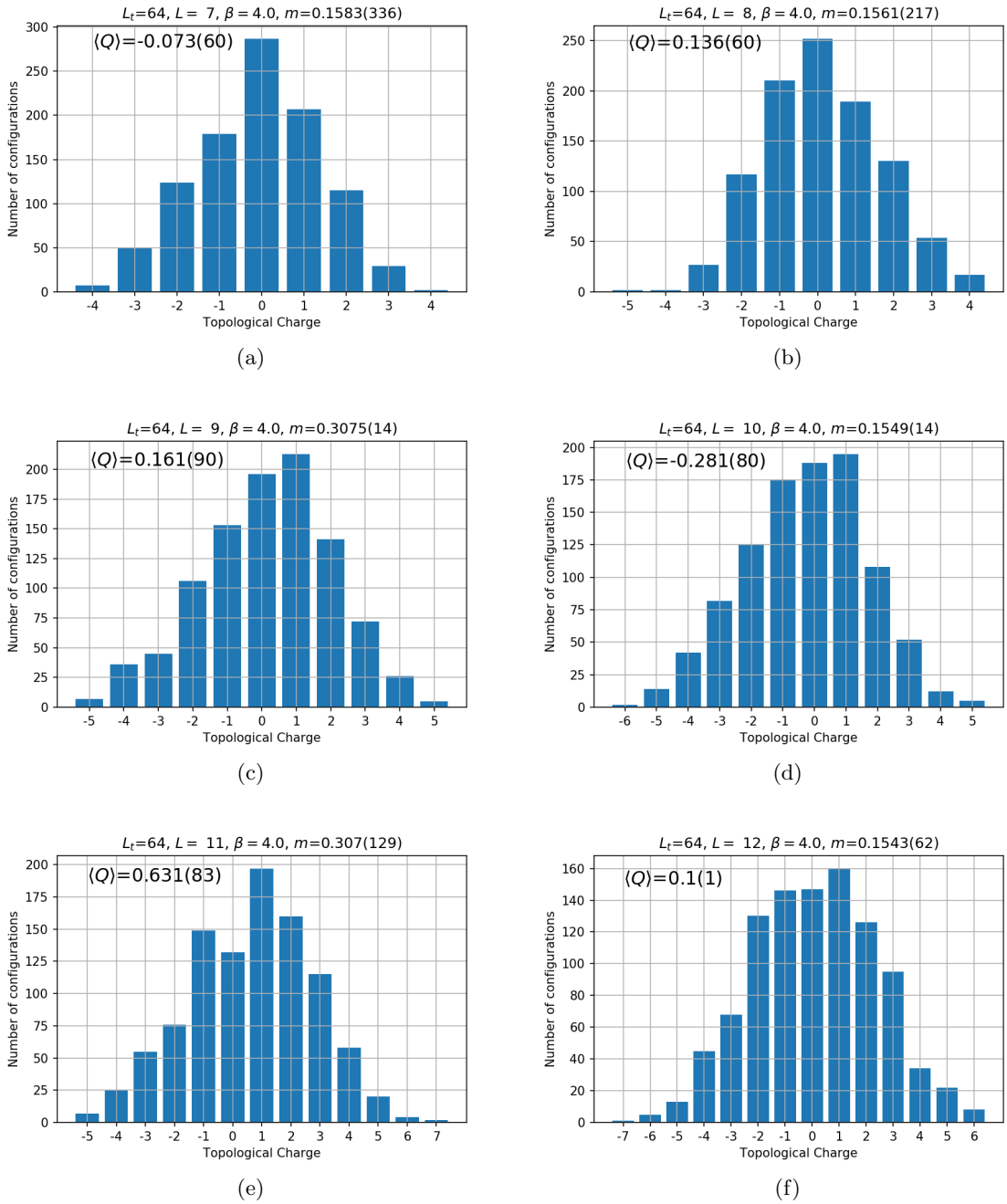

Figure 4.10: Topological charge distribution for different lattices and fermion mass, $\beta = 4$.

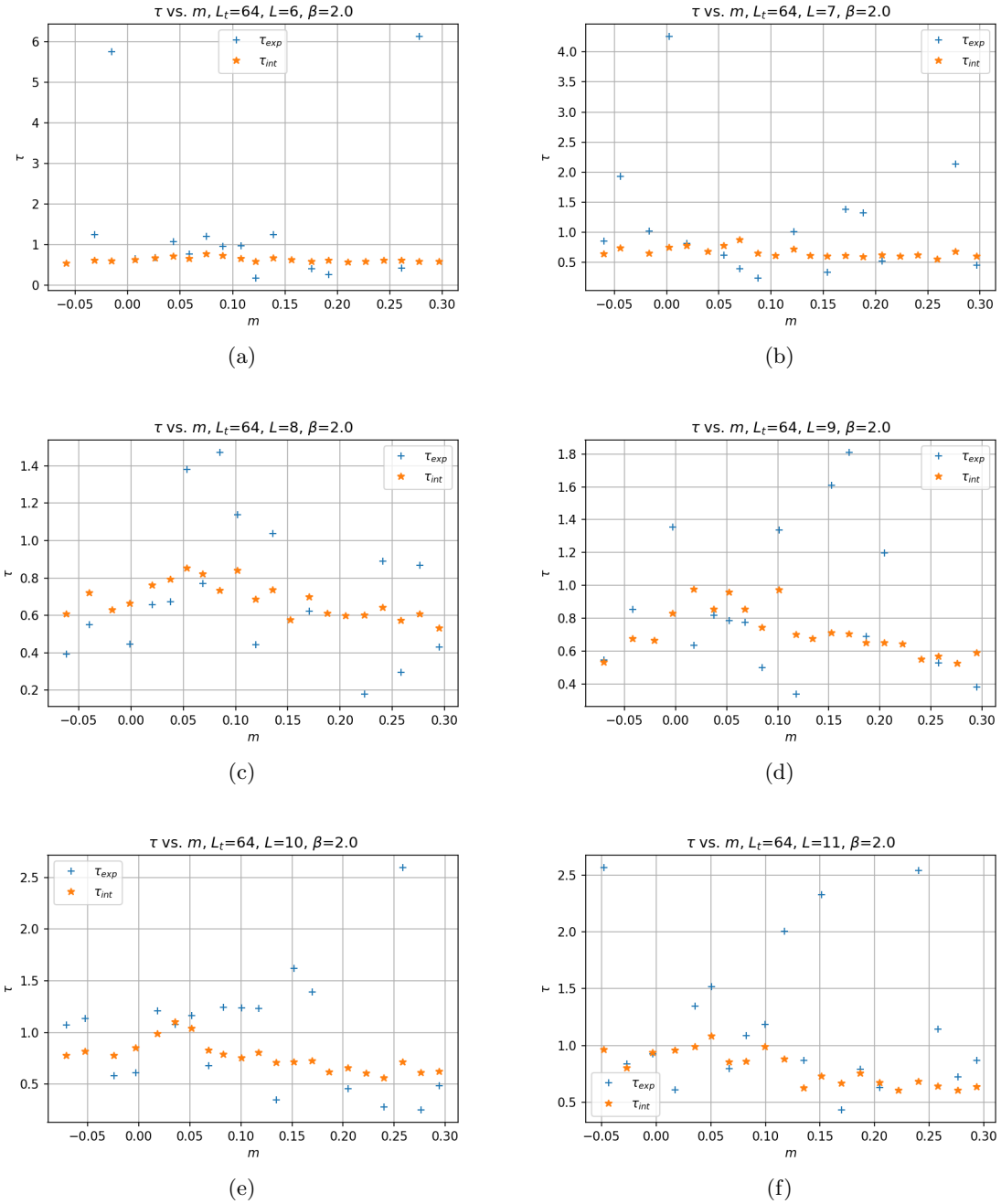

(a) (b) (c) (d) (e) (f)

Figure 4.11: Exponential and integrated autocorrelation time of the topological charge for different lattices, $\beta = 2$.

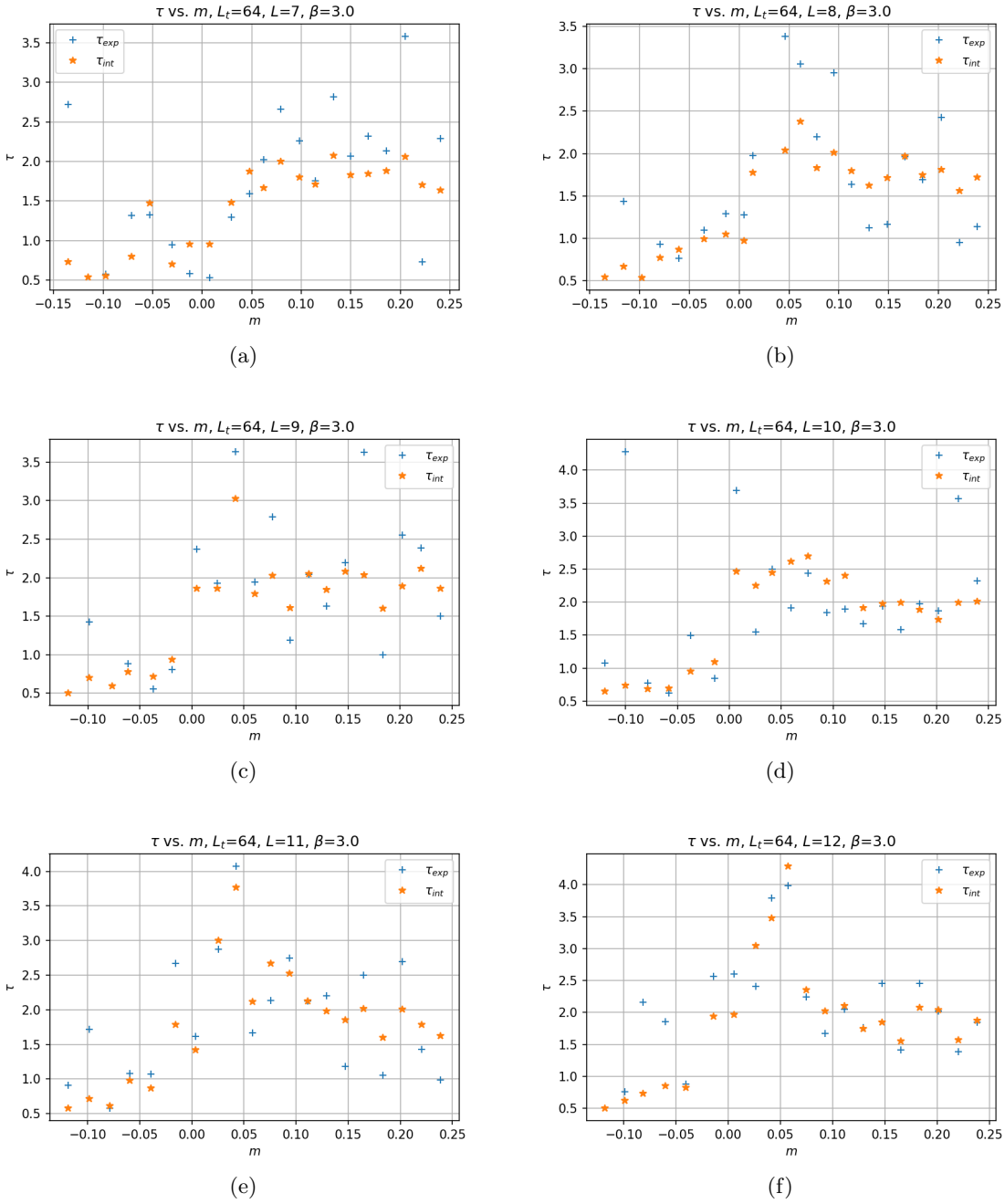

(a) (b) (c) (d) (e) (f)

Figure 4.12: Exponential and integrated autocorrelation time of the topological charge for different lattices, $\beta = 3$.

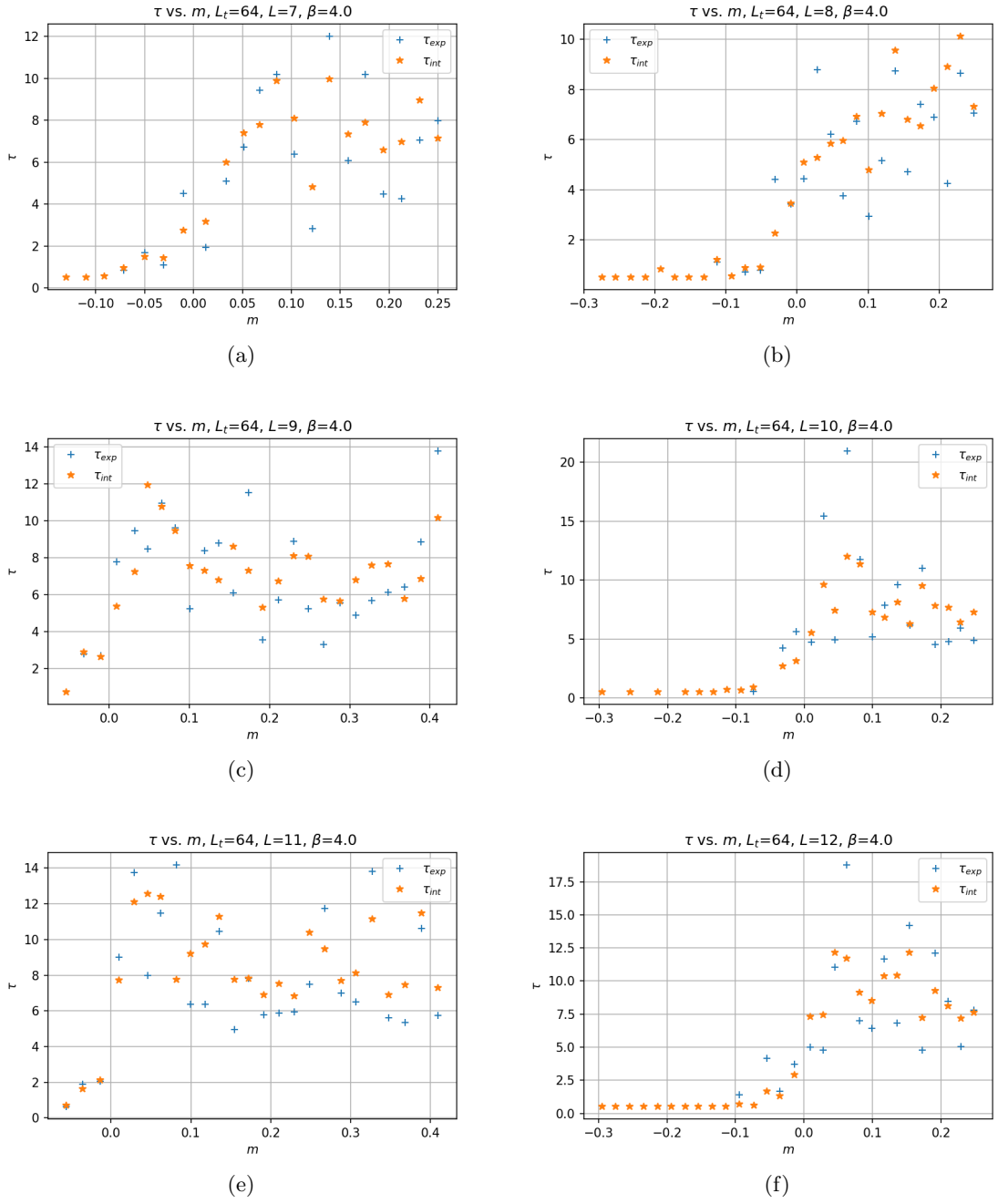

(a) (b) (c) (d) (e) (f)

Figure 4.13: Exponential and integrated autocorrelation time of the topological charge for different lattices, $\beta = 4$.

Bibliography

[1] P.A. Zyla et al. Review of Particle Physics. *Prog. Theor. Exp. Phys.*, 2020:083C01, 2020.

[2] A. Pich. Chiral perturbation theory. *Rept. Prog. Phys.*, 58:563–610, 1995.

[3] S. Scherer and M. R. Schindler. *A Primer for Chiral Perturbation Theory*. Springer, 2012.

[4] H. Leutwyler. Chiral perturbation theory. *Scholarpedia*, 7:8708, 2012.

[5] J. Gasser and H. Leutwyler. Light Quarks at Low Temperatures. *Phys. Lett. B*, 184:83–88, 1987.

[6] P. Hasenfratz and H. Leutwyler. Goldstone Boson Related Finite Size Effects in Field Theory and Critical Phenomena With O(N) Symmetry. *Nucl. Phys. B*, 343:241–284, 1990.

[7] J. Gasser and H. Leutwyler. Thermodynamics of chiral symmetry. *Phy. Lett. B*, 188:477–481, 1987.

[8] M. Golterman. Applications of chiral perturbation theory to lattice QCD. In *Les Houches Summer School: Session 93: Modern perspectives in lattice QCD: Quantum field theory and high performance computing*, pages 423–515, 2009.

[9] M. Abramowitz and I. A. Stegun. *Handbook of Mathematical Functions with Formulas, Graphs, and Mathematical Tables*. Dover, 1964.

[10] H. Leutwyler. Energy Levels of Light Quarks Confined to a Box. *Phys. Lett. B*, 189:197–202, 1987.

[11] S. Aoki et al. Review of lattice results concerning low-energy particle physics. *Eur. Phys. J. C*, 77:112, 2017.

[12] A. Bazavov et al. Results for light pseudoscalar mesons. *PoS*, LATTICE2010:074, 2010.

[13] R. Arthur et al. Domain wall QCD with near-physical pions. *Phys. Rev. D*, 87:094514, 2013.

[14] E. Follana, C. T. H. Davies, G. P. Lepage, and J. Shigemitsu. High-Precision Determination of the π, K, D, and D_s Decay Constants from Lattice QCD. *Phys. Rev. Lett.*, 100:062002, 2008.

[15] W. Bietenholz, M. Göckeler, R. Horsley, Y. Nakamura, D. Pleiter, P.E.L. Rakow, G. Schierholz, and J.M. Zanotti. Pion in a box. *Phy. Lett. B*, 687:410–414, 2010.

[16] P. Hasenfratz and F. Niedermayer. Finite size and temperature effects in the AF Heisenberg model. *Z. Phys. B*, 92:91, 1993.

[17] P. Hasenfratz. The QCD rotator in the chiral limit. *Nucl. Phys. B*, 828:201–214, 2010.

[18] N. D. Mermin and H. Wagner. Absence of Ferromagnetism or Antiferromagnetism in One- or Two-Dimensional Isotropic Heisenberg Models. *Phys. Rev. Lett.*, 17:1133–1136, 1966.

[19] P. C. Hohenberg. Existence of Long-Range Order in One and Two Dimensions. *Phys. Rev.*, 158:383–386, 1967.

[20] S. R. Coleman. There are no Goldstone bosons in two-dimensions. *Commun. Math. Phys.*, 31:259–264, 1973.

[21] A. V. Smilga and J. J. M. Verbaarschot. Scalar susceptibility in QCD and the multiflavor Schwinger model. *Phys. Rev. D*, 54:1087–1093, 1996.

[22] C. Gattringer and C. B. Lang. *Quantum Chromodynamics on the Lattice*. Springer, 2010.